Electron energy-loss spectroscopy fine structure of the Cu $L_{2,3}$ ionization edge in substitutional Cu-Ni alloys

2001 J. Phys.: Condens. Matter 13 3791

(http://iopscience.iop.org/0953-8984/13/16/309)

INSTITUTE OF PHYSICS PUBLISHING JOURNAL OF PHYSICS: CONDENSED MATTER

J. Phys.: Condens. Matter **13** (2001) 3791–3803 www.iop.org/Journals/cm PII: S0953-8984(01)16911-0

Electron energy-loss spectroscopy fine structure of the Cu $L_{2,3}$ ionization edge in substitutional Cu–Ni alloys

Cécile Hébert[1], Sylvain Clair[1], Christoph Eisenmenger-Sittner[1], Herwig Bangert[1], Bernard Jouffrey[2] and Peter Schattschneider[1]

[1] Institut für Angewandte und Technische Physik, Technische Universität Wien, Wiedner Hauptstraße 8–10, 1040 Wien, Austria
[2] LMSS-Mat, École Centrale Paris, Grande Voie des Vignes, 92295, Châtenay Malabry, France

Received 5 September 2000, in final form 15 February 2001

Abstract

We present a study of Cu–Ni alloys with different Ni concentrations using electron energy-loss spectroscopy in order to establish a relationship between the Ni concentration and the energy-loss near-edge structures of the Cu L_3 ionization edge. The experimental results are compared with *ab initio* band-structure calculations made with the WIEN97 and TELNES packages. We found excellent agreement between experiment and simulation making use of a supercell for modelling the Cu–Ni alloy. We were able to interpret the evolution of the fine structures in terms of local and global composition.

1. Introduction

Electron energy-loss spectroscopy (EELS) of the fine structure of ionization edges (ELNES, standing for 'energy-loss near-edge structure') probes the unoccupied states above the Fermi level. As such, it has long been used for the investigation of the electronic structure of materials in the solid state. Since the neighbourhood of the atom to be ionized defines the density of states at the actual site, ELNES can be used as a fingerprinting method to distinguish different chemical environments [1–3]. It has been realized that for the majority of problems, fingerprint techniques or intuitive arguments are not sufficient; rather, simulation of the spectral shape should allow cross-checks of models with experiment. Modern methods of simulation of ELNES employ density functional theory (DFT) as a tool for obtaining single-electron wave functions for the final state or use a multiple-scattering approach combined with a realistic scattering potential [4, 5].

The CuNi system has been widely studied as it is well suited for theoretical and experimental investigations. CuNi forms a face-centred-cubic (fcc) random solid solution over the entire concentration range and the lattice parameters of the two components only differ by 2.5%. As such it provides an ideal test case for theory applying to random substitutional alloys.

A large proportion of the electronic properties calculations have been carried out in the framework of the coherent potential approximation (CPA [6, 7]) and its derivatives and

improvements. See e.g. the early works of Kirkpatrick *et al* and of Stocks *et al* [8, 9]. Richter *et al* introduced the LCAO approach of the CPA [10]. More recently, Karolik and Golub calculated the density of electronic states, the electronic heat capacity and the coefficient of absolute-electron-diffusion thermoelectric power using the augmented-plane-wave method in the virtual-crystal approximation and compared them with experimental findings [11]. All of these works have been done within approximations where some properties of the random alloy are replaced by averages of the properties of the different components. Sommers *et al* calculated the band structure of CuNi by means of a KKR program using supercells of 1, 2, 4 and 8 atoms with different configurations which allows one to distinguish the atoms by means of their local environment [12].

The increasing power of computers allows us now to carry out calculations on big supercells also using relatively time-consuming methods like the FLAPW (full-potential linearized augmented-plane-wave) method. The aim of the present paper is to study the effect of introducing disorder in a CuNi crystal and compare simulated EELS spectra with experiments.

We concentrated on the Cu L edge because the Ni L edge exhibits strong white lines caused by the incompletely filled 3d band, making the fine structures in the edge less visible. Additionally, the CuNi alloy becomes magnetic when containing more than 67% Ni, making the simulations more complicated (but still possible [13]); thus, we wanted to restrict consideration to alloys with up to 50% Ni. Cu has a nearly filled d band. No correlation effects of the d holes are expected to complicate the simulations. The Cu L_3 ionization edge is positioned at an energy loss of 931 eV, the Cu L_2 at 951 eV, so the L_2 edge is not concerned in the fine structure (the first 20–30 eV above the edge) of the $L_{2,3}$ edge. The Cu L edge exhibits three maxima whose positions and relative heights change when the Ni concentration changes. We will show that the ELNES can be predicted successfully. Furthermore, a simple rule of thumb is derived that relates the positions of the maxima to the *global* concentration, and their heights to the *local* concentration of Ni atoms in the vicinity of an ionized Cu atom.

2. Conventions

We studied three alloys with respectively 0% ($x = 0$), 25% ($x = 0.25$) and 50% Ni ($x = 0.5$). All of the concentrations given in this paper are nickel concentrations.

As we only studied the Cu L_3 edge, we always take a Cu as the central atom.

N_{M}^{x} is the number of first neighbours of type M in the alloy of Ni concentration x. $\bar{N}_{\mathrm{M}}^{x}$ is the average of the number of first neighbours of type M over the whole cell.

3. Calculations

3.1. Theory

Band-structure methods are particularly suited to simulations of ELNES in crystals. They proceed from a perturbation theoretical first-order expression for the double-differential scattering cross-section for inelastic electron scattering.

For the present calculations, the WIEN97 code [14, 15], a FLAPW program, was used. The TELNES module is used in particular for calculation of angle-resolved EELS spectra [16]. TELNES derives the dynamic form factor (DFF) by an explicit evaluation of the matrix elements squared, thus circumventing the usual restriction of the dipole selection rule.

The DFF relates to the inelastic differential scattering cross-section as follows:

$$\frac{\partial^2\sigma}{\partial\Omega\,\partial E} = \frac{4\gamma^2}{a_0^2 q^4}\frac{k_f}{k_i}\,\mathrm{DFF}(\vec{q}, E) \tag{1}$$

where $\vec{k}_i$ and $\vec{k}_f$ are the initial and final wave vectors of the fast electron and $\vec{q} = \vec{k}_i - \vec{k}_f$ is the momentum transfer. a_0 is the Bohr radius and $\gamma = \sqrt{(1-\beta^2)}$ the relativistic factor.

For a polycrystalline specimen, i.e. for arbitrary orientation of crystallites, the integral over all directions under neglect of dynamical diffraction leads to [16, 17]

$$\mathrm{DFF}(\vec{q}, E) = o_l \sum_{\lambda=0}^{\infty} \sum_{l'=|l-\lambda|}^{l+\lambda} \chi_{l'}^{t}(\varepsilon')(2\lambda+1)\begin{pmatrix} l & \lambda & l' \\ 0 & 0 & 0 \end{pmatrix}^2 \langle j_\lambda(q)\rangle_{n\varepsilon' ll'}^2 \tag{2}$$

for the DFF. Here $o_l = 2(2l+1)$ is the statistical occupation number of the initial state, and $\chi_{l'}^{t}(\varepsilon')$ is the partial density of final states for angular momentum l' at atom t and for the energy ε'; the sum is over the transfer of angular momentum λ in the interaction and over all possible final angular momenta l'. Also,

$$\langle j_\lambda(q)\rangle_{n\varepsilon' ll'} = \int u_{nl}(r)\, j_\lambda(qr) u_{\varepsilon' l'}(r) r^2\,\mathrm{d}r \tag{3}$$

is the matrix element of the spherical Bessel function of order λ between the radial parts u_{nl} of the initial and $u_{\varepsilon' l'}$ of the final state.

3.2. Neighbours in single cells and supercells

The input data to WIEN97 are those describing the unit cell of a crystal (space group and positions of atoms). We built five cells in order to simulate the following alloys: pure Cu, 25% Ni and 50% Ni. The calculations for the pure Cu, 25% Ni and 50% Ni were made with a simple cell with four atoms per unit cell, and calculations for two '$2 \times 2 \times 1$' supercells containing 16 atoms were also made for $x = 0.25$ and $x = 0.5$.

In a perfect random binary alloy with components A and B with the concentrations x_A and x_B respectively ($x_\mathrm{A} + x_\mathrm{B} = 1$) and with N first neighbours, the probability of having N_A atoms of type A as first neighbours is given by

$$f_{x_\mathrm{B}}(N_\mathrm{A}) = x_\mathrm{B}^{N-N_\mathrm{A}}(1-x_\mathrm{B})^{N_\mathrm{A}}\frac{N!}{N_\mathrm{A}!(N-N_\mathrm{A})!}. \tag{4}$$

In the case of CuNi, which has $N = 12$ first neighbours, the probability of having N_Cu copper atoms as first neighbours is plotted versus N_Cu^x for $x = 0.25$ and $x = 0.5$ in figure 1.

Thus, the average of the number of Cu first neighbours is given by $\bar{N}_\mathrm{Cu}^x = N(1-x)$, which leads to $\bar{N}_\mathrm{Cu}^{0.5} = 6$ and $\bar{N}_\mathrm{Cu}^{0.25} = 9$.

An alloy made by repeating fcc single cells is inevitably a superstructure—for example, in the case of 50% Ni, a stack of alternating pure Cu and pure Ni planes (figure 2) [18].

In the single cell where either one or two Cu atoms are replaced by Ni atoms, all of the Cu atoms have the same number of Cu/Ni first neighbours. In the 50% Ni alloy, each Cu is surrounded by four Cu and eight Ni (figure 2); thus $\bar{N}_\mathrm{Cu}^{0.5} = 4$ (instead of 6, as in the ideal random crystal). For the 25% Ni alloy, $\bar{N}_\mathrm{Cu}^{0.25} = 8$ (instead of 9).

To avoid the superstructure, it is necessary to build a supercell. As the computation time roughly increases as the third power of the number of inequivalent atoms in the unit cell, we restricted the calculation to a supercell with 16 atoms in it. We choose a $2 \times 2 \times 1$ supercell rather than a $\sqrt{2} \times \sqrt{2} \times 2$ one, because the possibility of selecting atoms with different neighbours is increased.

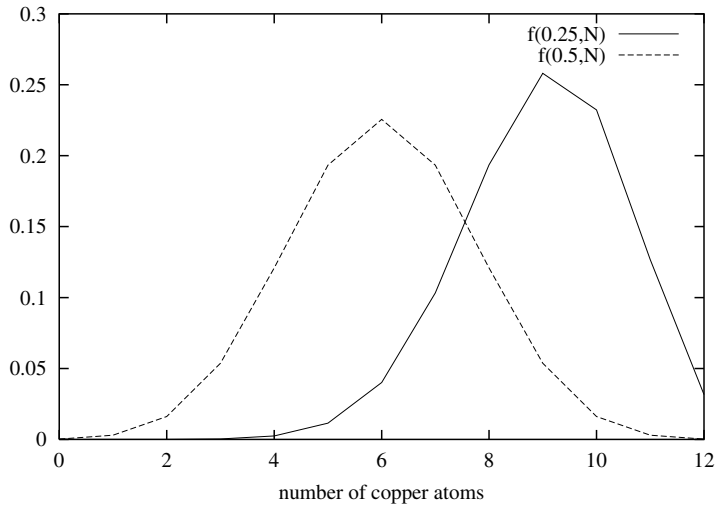

Figure 1. The probability of having N_{Cu}^{x} copper atoms as first neighbours as a function of N_{Cu}^{x} for $x = 0.25$ (solid line) and $x = 0.5$ (dashed line) in a perfectly random alloy.

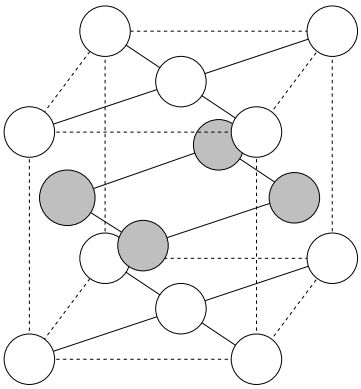

Figure 2. A 50% single cell; repetition of this leads to a stack of (100) planes of pure Cu and Ni.

The atomic positions in a supercell are chosen in such a way that the statistics over the first neighbours tends to the ideal statistics of a perfect random alloy. The $2 \times 2 \times 1$ supercells can be represented by two layers each containing eight atoms. Figures 3 and 4 show the supercells and the corresponding probability of having N_{Cu}^{x} copper atoms as first neighbours compared with the ideal probability for $x = 0.25$ and $x = 0.5$, respectively.

The distribution obtained then is still far from perfect, especially for $x = 0.5$, but as we will see later, the improvement in the calculation is very important. For the two supercells, the average numbers of Cu atoms as first neighbours are $\bar{N}_{\mathrm{Cu}}^{0.25} = 9$ and $\bar{N}_{\mathrm{Cu}}^{0.5} = 5.25$ which are closer to the mean values for a perfect random alloy in comparison with the single cell.

3.3. Inputs for WIEN97

All of the calculations have been performed with a muffin-tin radius of 2.1 atomic units for both Cu and Ni. The calculation is converged in terms of plane-wave cut-off and k-mesh.

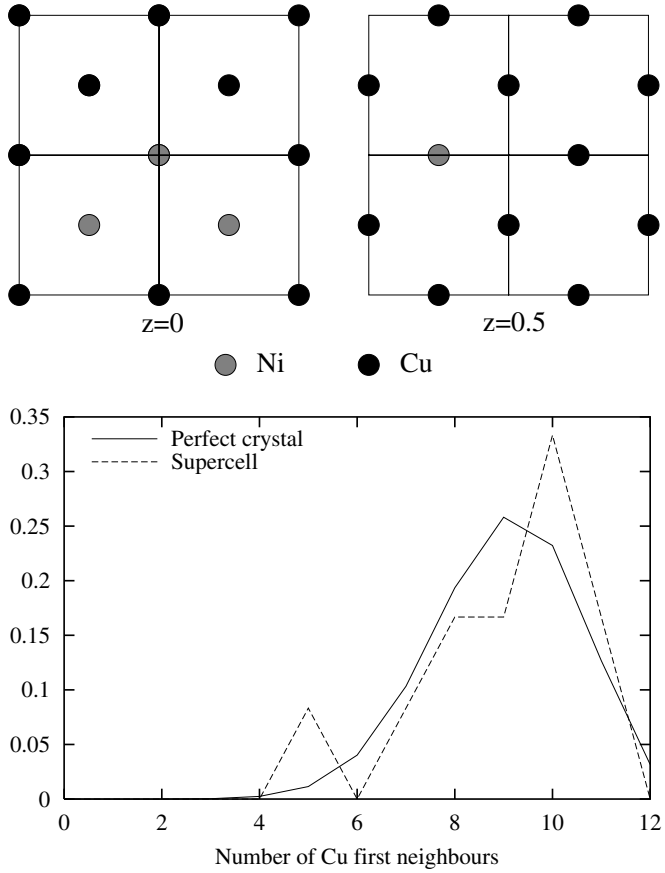

Figure 3. The supercell for the 25% Ni alloy and the probability of having $N_{\mathrm{Cu}}^{0.25}$ copper atoms as first neighbours compared with the probability calculated for a perfect random alloy of the same composition. The two 'layers', each containing eight atoms and situated respectively at $z = 0$ and $z = 0.5$ in the supercell, are represented separately to provide a better understanding.

The k-mesh is 8000 k-points in the whole BZ for the single cells and 2000 k-points for the supercells. Spectra have been calculated with a full k-mesh in order to avoid small artifacts due to different symmetries of the single cells and supercells.

The spectra were broadened with a Gaussian of FWHM 1.8 eV in order to account for instrumental resolution. The core-hole lifetime broadening of 0.4 eV [19] was neglected. The quite complicated energy-dependent excited lifetime broadening was also neglected, as the approximation proposed by Muller *et al* [20] is only valid in the immediate vicinity of the edge (5–7 eV above the Fermi level) where the broadening remains small; thereafter the approximation dramatically overestimates the broadening [21].

4. Experiment

The specimens were produced in a magnetron sputtering system. They were 50 nm thick, polycrystalline, with grains of about 10 nm. The ELNES spectra were taken on a 200 kV Philips CM20 microscope equipped with a Gatan 666 PEELS.

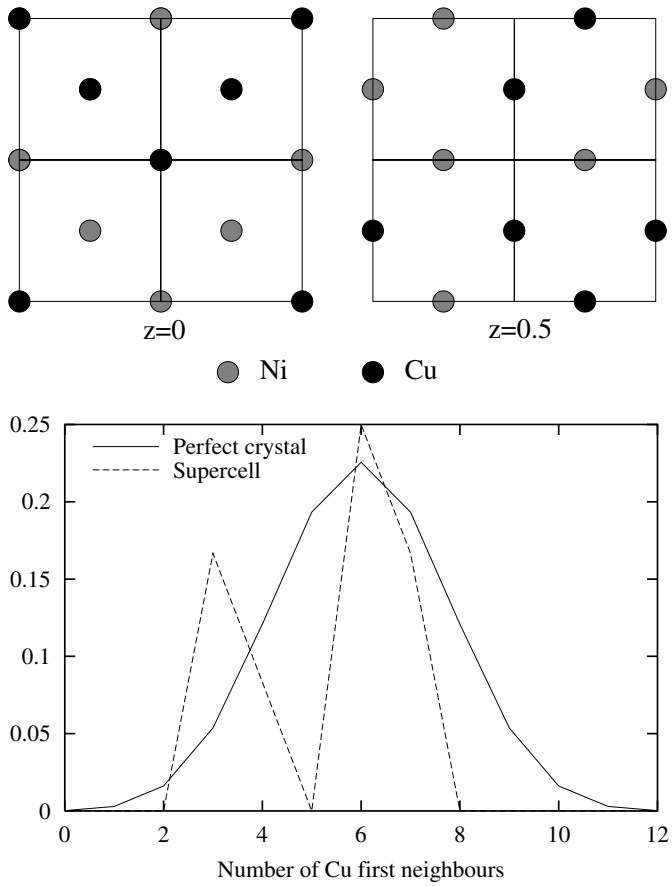

Figure 4. The supercell for the 50% Ni alloy and the probability of having $N_{\mathrm{Cu}}^{0.5}$ copper atoms as first neighbours compared with the probability calculated for a perfect random alloy of the same composition. The two 'layers', each containing eight atoms and situated respectively at $z = 0$ and $z = 0.5$ in the supercell, are represented separately to provide a better understanding.

The spectra were taken in image mode with a spectrometer entrance aperture of 3 mm. The signal was integrated over a large range of different orientations. The spectra were deconvoluted from multiple scattering and from the point-spread function, and the background removed using standard procedures [22].

5. Results

5.1. Local and global composition

Figures 5 and 6 show the evolution of the spectra for the different concentrations for the experiment and for the simulations with the single cell and supercell. It is evident that the simulation made with supercells differs significantly from that for the single cells and represents better the evolution of the three peaks when more Ni is added to the alloy.

For more details, the spectra can be analysed in terms of the relative heights and positions of the three peaks.

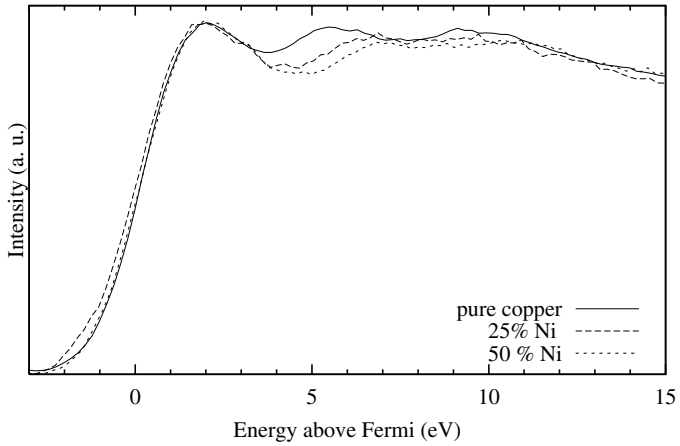

Figure 5. The experimental Cu L_3 edge recorded on a Philips CM20 UT 200 kV microscope equipped with a Gatan PEELS for different Ni concentrations.

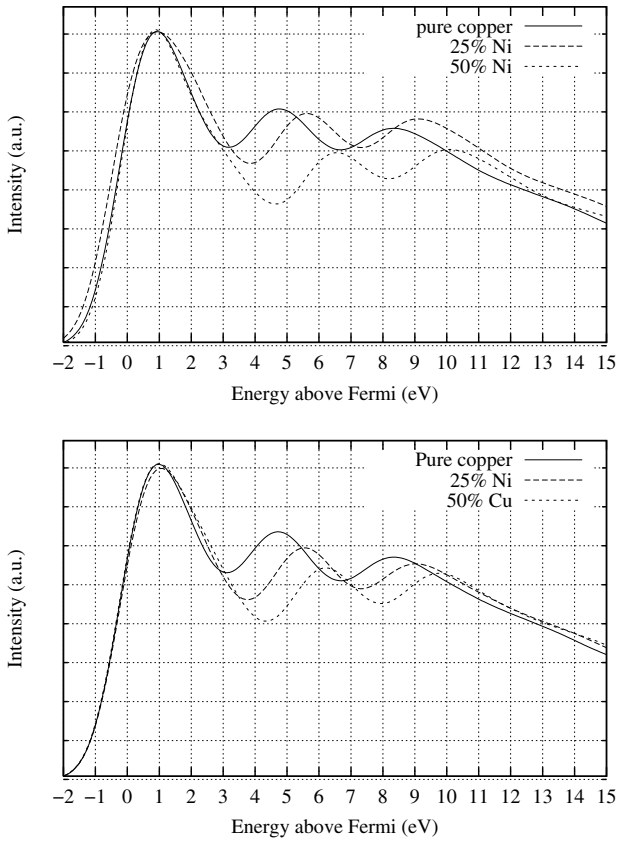

Figure 6. Simulated Cu L_3 edges for different nickel concentrations. At the top: the simulations done using a single cell. At the bottom: the simulations done within the supercells presented in figures 3 and 4.

Figure 7 shows a comparison of the relative positions of the three peaks as functions of concentration. The experimental peak positions are in good agreement with those predicted by simulations and there is no evidence that the calculated peak positions are better when using a supercell. From the peak position, one could conclude that the simulation can be done using a single cell.

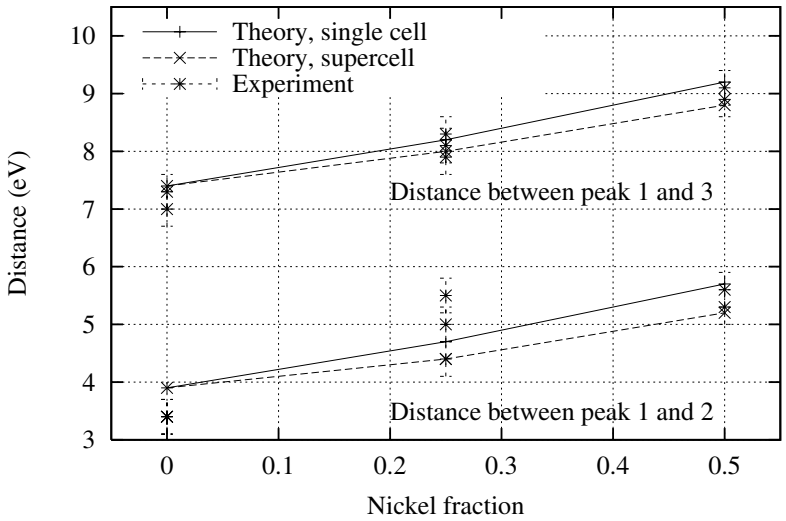

Figure 7. Distances in eV between peaks 1 and 2 and peaks 1 and 3 for the single cell and for the supercell compared with experiments. The single cell and the supercells give similar and good results.

From figures 5 and 6 it is evident that the height of the first peak is overestimated in the simulation. This is a result of the imperfectly screened core hole [23]. It is generally admitted that in metals, the core hole left by the excited electron is quickly screened by the valence electrons and thus is not visible in the experimental spectrum, in contrast to what happens in insulators [24–26]. However, this simple rule is not always obeyed and the core hole can also be partially seen in metals. A core-hole calculation is beyond the scope of this paper. (It would require eight scf cycles for the 50% Ni supercell and twelve scf cycles for the 25% Ni supercell.)

Therefore, the calculated relative peak heights were all normalized to the experimental relative height for pure copper assuming that the core hole affects all alloys in the same way; this procedure should remove the core-hole effect.

The results are shown in figure 8 and it is clear that the single-cell and supercell calculations strongly differ and that the supercell calculations fit the experiment much better.

From those results, it is possible to conclude that the peak position is only affected by the global composition—this means by the average Ni composition over the whole cell—whereas the peak height depends on the local composition—this means the number of Cu and Ni atoms surrounding one particular atom.

6. First and second neighbours

One benefit of the supercell method is that it allows one to compare the spectra obtained from atoms with different local environments. Figure 9(a) compares two atoms in the 25% Ni

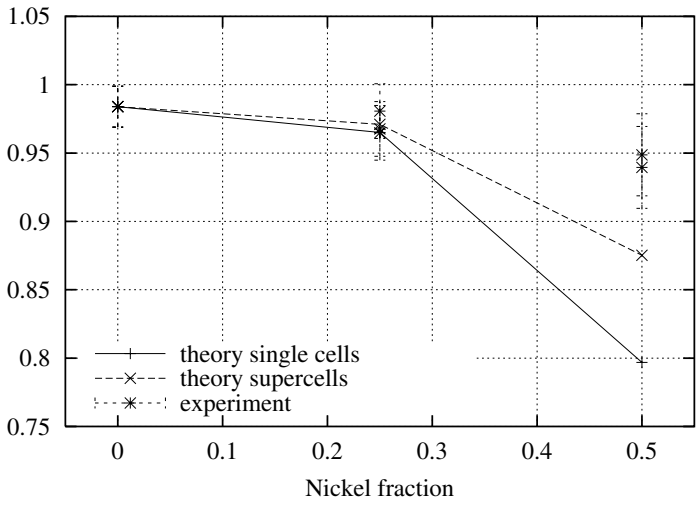

(a)

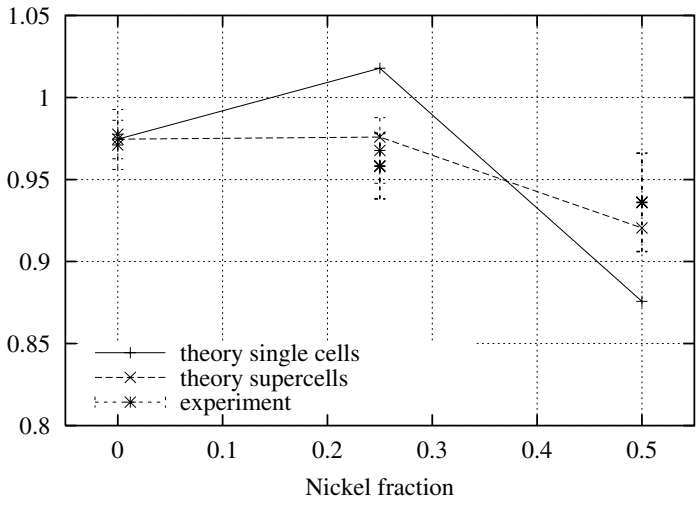

(b)

Figure 8. (a) Relative heights of peaks 1 and 2, $P(2)/P(1)$. (b) Relative heights of peaks 1 and 3, $P(3)/P(1)$. Comparison of the heights of the three peaks shows that the supercell simulation represents the evolution of the relative height as a function of the nickel concentration much better. The theoretical values have been normalized by the theoretical relative height over the experimental relative height for pure copper.

supercell with different first neighbours but identical second and similar third neighbours. The peak position is not really affected but the peak heights differ strongly, as one could expect from the preceding results. Figure 9(b) shows two spectra from atoms where only the second neighbours are different. They are very similar, so one can conclude that only the first neighbours play an important role in the spectrum shape.

Figure 10(a) compares two atoms of the 25% Ni cell—one with a Ni-rich local environment and one with a Cu-rich local environment—with the pure copper cell. Again, it is evident that the atom with the nearly pure Cu environment has nearly the same peak heights as the one

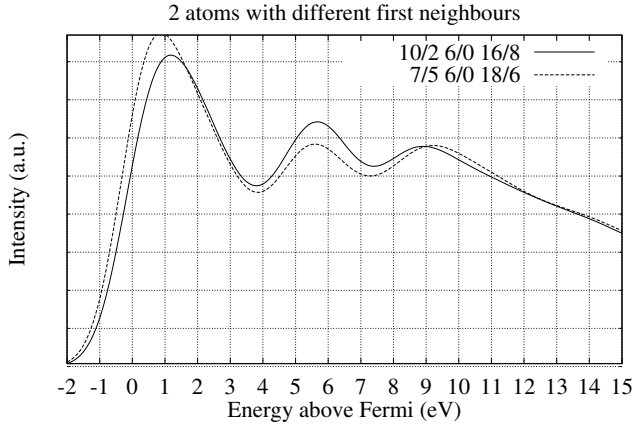

(a)

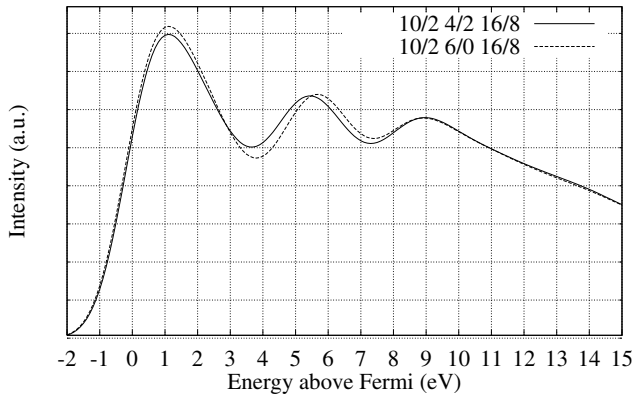

(b)

Figure 9. (a) Two atoms with different first neighbours. (b) Two atoms with different second neighbours. The effect of the local environment on the ELNES in the 25% Ni supercell. Only the first neighbours have an important influence. The numbers of first, second and third neighbours are given as follows: Cu first neighbours/Ni first neighbours, Cu second neighbours/Ni second neighbours, Cu third neighbours/Ni third neighbours; thus '10/2 6/0 16/8' means that 10 first, 6 second and 16 third neighbours are Cu atoms.

in pure copper but the peak positions are very different. In contrast, the two atoms with the same global composition have nearly the same peak positions, but the heights differ strongly. A comparison of two spectra from two atoms from the 50% Ni and 25% Ni supercells with similar local environments shows the same behaviour (figure 10(b)).

7. Density of states

As can be seen in figure 11, a change in the global composition produces a shift of the density of states if more nickel is added to the alloy; the maximum of the density of states tends to be at higher energies with respect to the Fermi energy, which is easy to understand: Ni tends to attract the electron from copper. The structures of the spectrum are therefore shifted to higher energies in the spectrum; thus the global composition influences the peak position.

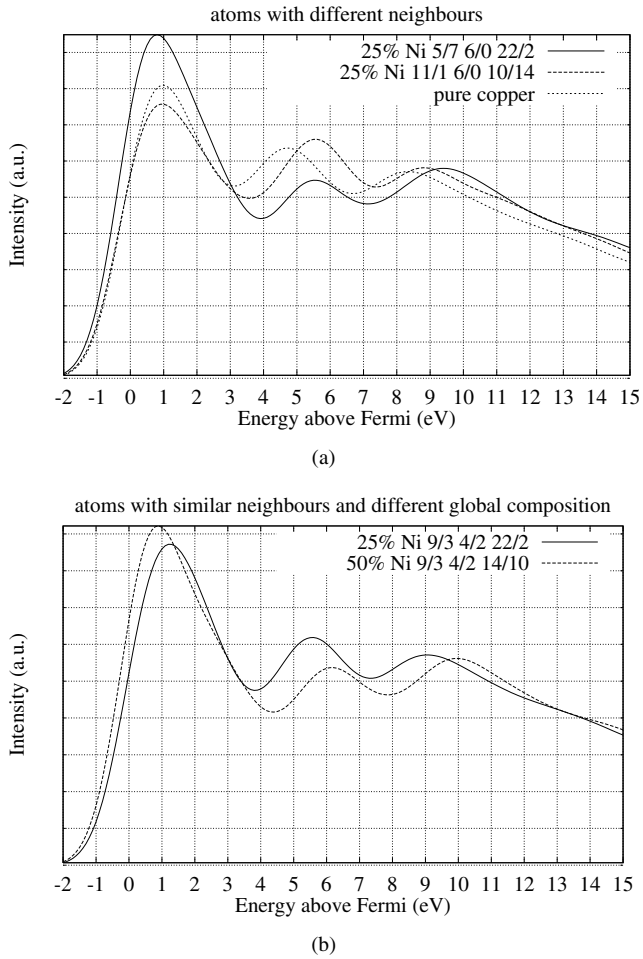

Figure 10. (a) Two atoms with different local environments compared with pure copper. (b) Two atoms with similar local compositions and different global compositions. Cu L_3 edges simulated for atoms with different local and global compositions. The global composition influences the peak position and the local composition the peak height. The numbers of first, second and third neighbours are given as follows: Cu first neighbours/Ni first neighbours, Cu second neighbours/Ni second neighbours, Cu third neighbours/Ni third neighbours; thus '5/7 6/0 22/2' means that 5 first, 6 second and 22 third neighbours are Cu atoms.

Once the global composition is fixed, the structures of the DOS of the different atoms of the alloy are fixed at the same energy: thus the peak position is fixed. The local composition influences the peak height via the locally different charge transfer.

8. Conclusions

The ELNES of the copper L_3 edge in several Cu–Ni alloys have been studied experimentally as well as with computer simulations. The good agreement between the results encourages further use of the simulation and analysis of the individual atoms depending on their local environment. The simulation then gives information which is not available in the experiment. A relatively small supercell of 16 atoms is enough for obtaining good agreement between

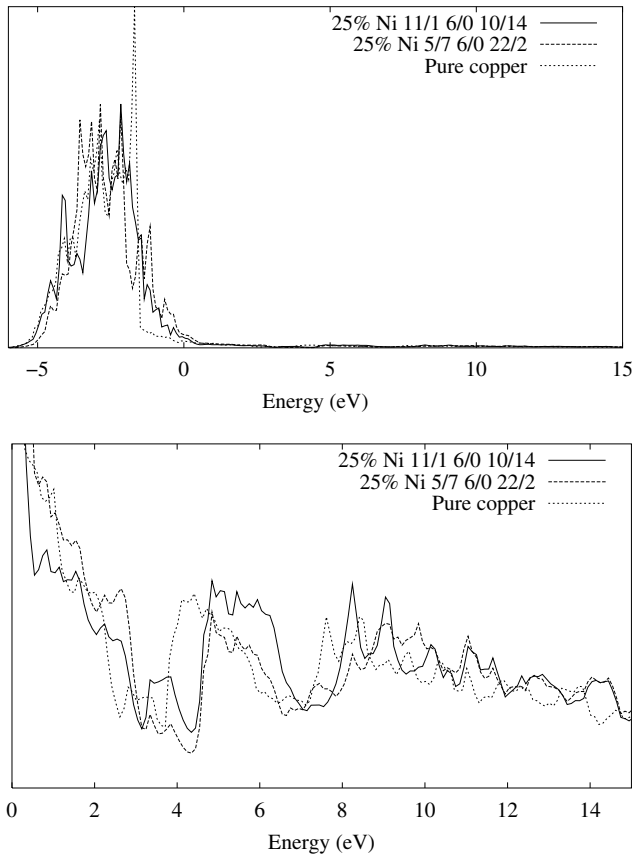

Figure 11. The partial d DOS for two atoms with different first neighbours compared with the d DOS in pure copper. The Fermi energy is set at 0 eV. The numbers of first, second and third neighbours are given as follows: Cu first neighbours/Ni first neighbours, Cu second neighbours/ Ni second neighbours, Cu third neighbours/Ni third neighbours; thus '11/1 6/0 10/14' means that 11 first, 6 second and 10 third neighbours are Cu atoms.

experiment and simulations. We were able to show that the first impression that the peak position is related to the global composition and the peak height to the local composition can be confirmed and explained by interpreting the local d-projected density of states. In view of the minute variations in the unoccupied DOS in the CuNi system, ELNES must be a very sensitive method for analysing the electronic structure of materials.

Acknowledgments

The financial support of the Austrian Science Fund (project P14038-PHY) and of the Hochschuljubiläumsfonds der Stadt Wien is gratefully acknowledged.

References

[1] Bruley J, Keast V J and Williams D B 1996 *J. Phys. D: Appl. Phys.* **29** 1730
[2] Colliex C and Jouffrey B 1972 *Phil. Mag.* **25** 491
[3] Krivanek O L, Disko M M, Taftø J and Spence J C H 1982 *Ultramicroscopy* **9** 249

[4] Rez P, Bruley J, Brohan P, Payne M and Garvie L A J 1995 *Ultramicroscopy* **59** 159
[5] Rez P, Alvarez J R and Pickard C 1999 *Ultramicroscopy* **78** 175
[6] Soven P 1967 *Phys. Rev.* **156** 809
[7] Velický B, Kirkpatrick S and Ehrenreich H 1968 *Phys. Rev.* **175** 747
[8] Kirkpatrick S, Velický B and Ehrenreich H 1970 *Phys. Rev.* B **1** 3250
[9] Stocks G M, Willams R W and Faulkner J S 1971 *Phys. Rev.* B **4** 4390
[10] Richter R, Eschrig H and Velický B 1987 *J. Phys. F: Met. Phys.* **17** 351
[11] Karolik A S and Golub V M 1997 *Phys. Met. Metallogr.* **83** 461
[12] Sommers C B, Myron H W and Mueller F M 1980 *Solid State Commun.* **36** 411
[13] Hébert-Souche C, Bernardi J, Schattschneider P, Fidler J and Jouffrey B 2000 *Eur. Phys. J.* **9** 147
[14] Blaha P, Schwarz K and Sorantin P 1990 *Comput. Phys. Commun.* **59** 399
[15] Blaha P, Schwarz K and Luitz J 1999 *WIEN97, a Full Potential Linearized Augmented Plane Wave Package for Calculating Crystal Properties* (Vienna: Schwarz)
[16] Hébert-Souche C, Louf P-H, Blaha P, Nelhiebel M, Luitz J, Schattschneider P, Schwarz K and Jouffrey B 2000 *Ultramicroscopy* **83** 9
[17] Nelhiebel M, Louf P-H, Schattschneider P, Blaha P, Schwarz K and Jouffrey B 1999 *Phys. Rev.* B **59** 12 807
[18] Clair S, Hébert-Souche C, Eisenmenger-Sittner C, Bangert H and Schattschneider P 2000 *Proc. EUREM-XII* vol 2 (Brno: Czechoslovak Society for Electron Microscopy) pp 23–4
[19] Fuggle J C and Inglesfield J E (ed) 1992 *Unoccupied Electronic States* (Berlin: Springer)
[20] Muller D A, Singh D J and Silcox J 1998 *Phys. Rev.* B **57** 8181
[21] Hébert C, Kostner M and Schattschneider P 2000 *Proc. EUREM-XII* vol 3 (Brno: Czechoslovak Society for Electron Microscopy) pp 333–4
[22] Egerton R F 1986 *Electron Energy Loss Spectroscopy in the Electron Microscope* (New York: Plenum)
[23] Luitz J, Maier M, Hébert C, Schattschneider P, Blaha P, Schwarz K and Jouffrey B 2001 *Eur. Phys. J.* B at press
[24] Brydson R, Bruley J and Thomas J M 1988 *Chem. Phys. Lett.* **149** 343
[25] Lie K, Brydson R and Davock H 1999 *Phys. Rev.* B **59** 5361
[26] Mizoguchi T, Tanaka I, Yoshiya M, Oba F, Ogasawara K and Adachi H 2000 *Phys. Rev.* B **61** 2180